High-Contrast, Reversible Thermal Conductivity Regulation Utilizing the Phase Transition of Polyethylene Nanofibers

Teng Zhang[†] and Tengfei Luo[†,‡,*]

[†]Aerospace and Mechanical Engineering and [‡]Center for Sustainable Energy at Notre Dame, University of Notre Dame, Notre Dame, Indiana 46556, United States

ABSTRACT Reversible thermal conductivity regulation at the nanoscale is of great interest to a wide range of applications such as thermal management, phononics, sensors, and energy devices. Through a series of large-scale molecular dynamics simulations, we demonstrate a thermal conductivity regulation utilizing the phase transition of polyethylene nanofibers, enabling a thermal conductivity tuning factor of as high as 12, exceeding all previously reported values. The thermal conductivity change roots from the segmental rotations along the polymer chains, which introduce along-chain morphology disorder that significantly interrupts phonon transport along the molecular chains. This phase transition, which can be regulated by temperature, strain, or their combinations, is found to be fully reversible in the polyethylene nanofibers and can happen at a narrow temperature window. The phase change temperature can be further tuned by engineering the diameters of the nanofibers, making such a thermal conductivity regulation scheme adaptable to different application needs. The findings can stimulate significant research interest in nanoscale heat transfer control.

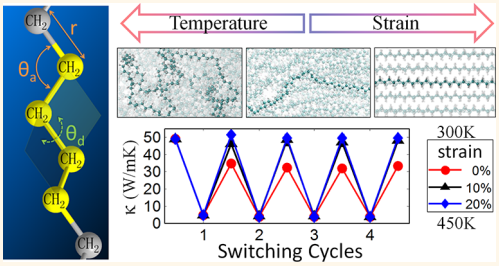

KEYWORDS: thermal switch · polyethylene nanofiber · molecular dynamics · phase transition

Macroscopic control of heat transfer, such as forced convection and thermal insulation, has existed for hundreds of years and played critical roles in our daily life. With the success of nanotechnologies, controlling thermal conductivity at the nanoscale becomes highly desirable for a wide range of applications such as thermal management of electronics, phononics, sensors, and energy storage and conversion. Efforts to control thermal conductivity using nanotechnologies have been made in the past. Supino *et al.*[1] employed a method using electrostatic control of thermal transport through a microstructure in and out of contact with its underlying substrate and achieved thermal conductivity tuning by a factor of 2. Other microscale thermal switches based on active or passive control of mechanical contact have also been proposed and studied.[2−5] Philip and co-workers[6] used magnetically polarizable nanofluids to tune thermal conductivity by controlling the linear aggregation length of the nanoparticles. This method changed thermal conductivity by a factor of 2. Through liquid−solid phase change of the main phase in nanofluids,[7] a change of thermal conductivity by 3 times between 3 and 25 °C was obtained due to the enhanced long-range particle aggregation when nanoparticles are squeezed to the grain boundaries in the frozen state. By manipulating the overlap of the outer and inner walls of a multiwall carbon nanotube using mechanical action, Chang *et al.*[8] achieved a thermal conductivity tunability of almost 7. These previous efforts either have limited tuning range or need complicated and high-cost devices. High-contrast thermal conductivity regulation using simple and cost-effective materials is desired for practical applications.

Polymers are inexpensive, readily available, and widely used in industry. Although amorphous polymers are known as thermal insulators with thermal conductivity ranging from 0.1 to 0.3 W/mK,[9] polymer fibers,[10] especially ultradrawn nanofibers[11] consisting of highly aligned polymer chains,

* Address correspondence to tluo@nd.edu.

Received for review April 7, 2013 and accepted August 13, 2013.

Published online August 13, 2013
10.1021/nn401714e

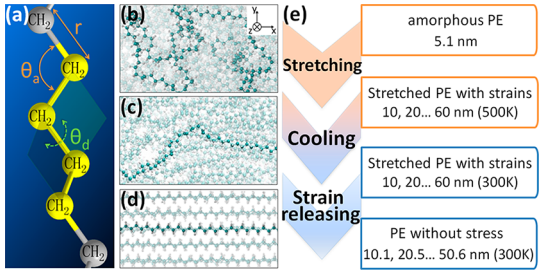

Figure 1. (a) Molecular backbone of a polyethylene chain. Due to the strong bond and angle interaction, bond length (r) and angle (θ_a) cannot have large variations. However, the weak dihedral angle (θ_d) can vary for a large range, leading to rotational disorder. (b–d) Snapshots of the morphology of polyethylene with different strains simulated in the ultradrawing process. (e) Flowchart of the ultradrawing process: amorphous polyethylene with an initial length of 5.1 nm in the x-direction is drawn to 1.96–10.77 times longer at 500 K. The structure is then cooled to 300 K, and the residual stress is released in a constant pressure simulation at 300 K.

are found to have thermal conductivity hundreds of times higher than that of their amorphous counterparts. The very high thermal conductivity roots from the one-dimensional phonon transport in which phonons can travel a long distance inside the straight polymer chains without attenuation.[12] The thermal conductivity of polymer fibers, however, is a strong function of their morphology.[13−17] It is found that segmental rotations along the polymer chains can significantly scatter phonons and thus reduce thermal conductivity.[13,15,16]

Phase change can be used to manipulate morphology and thus properties of materials. However, conventional phase change materials are usually "soft", having low phonon group velocity and large anharmonicity, and thus low thermal conductivity.[18] As a result, they offer little room for thermal conductivity tuning. The structural property of polyethylene chains is anisotropic. Although they are soft in the rotational degree of freedom, often indicated by the softness of the dihedral angle of the chain backbone (see θ_d in Figure 1a), both the bond stretching (r in Figure 1a) and bond bending (θ_a in Figure 1a) degrees of freedom are very stiff due to the strong carbon bonds.[19,20] This makes polyethylene nanofibers ideal platforms for thermal conductivity regulation. They can have very high intrinsic thermal conductivity due to the strong bond interactions, and disorder in the rotational degree of freedom can be manipulated easily to control phonon scattering and thus thermal conductivity. In this work, dramatic changes in morphology and dynamics are observed when the polyethylene chains transition from a highly ordered *all-trans* conformation to one with rotational disorders. We consider such a change a form of phase transition. In this work, using a series of large-scale molecular dynamics simulations, we demonstrate high-contrast, reversible thermal conductivity regulations utilizing this phase transition of polymer nanofibers.

All simulations in this work use 40 chains with each consisting of 400 CH_2 segments unless noted separately. Periodic boundary conditions are used in all three spatial directions. A fourth periodic condition[21] ties one end of a chain to the other end of its image, so that chains simulated are of infinite length. In practice, monodisperse ultrahigh molecular weight polyethylene (UHMWPE) approaches this limit.[22] More details of the simulations are presented in the Method section and sections 1 and 2 in the Supporting Information.

RESULTS AND DISCUSSION

We first show that the thermal conductivity of polyethylene can be modulated by the morphology change. We start with an amorphous polyethylene structure (see Figure 1b) and simulate the ultradrawing process, which is widely used to improve chain alignment and synthesize polymer fibers.[11,14,23] The optimized amorphous polyethylene supercell has a dimension of 51.06 Å × 89.75 Å × 126.22 Å at 300 K. The drawing process is simulated at 500 K by applying strains in the x-direction while allowing the dimensions in the y- and z-directions free to change. The strains are simulated by increasing the supercell dimension in the x-direction artificially. Eleven different draw ratios are studied. Here, draw ratio is defined as the ratio of the x-direction supercell length after straining to the initial length. After each draw ratio is achieved, the structure is cooled to 300 K. Then, an equilibration run in a constant number of atom, constant pressure, and constant temperature ensemble (NPT) at 300 K and 1 atm is performed to remove residual stress, optimize the simulation cell sizes, and obtain the stable structures at 300 K. Figure 1e depicts the flowchart of the simulated drawing process. The morphology of the polyethylene is found to be a strong function of the draw ratio (Figure 1b–d).[24−26] It is found that, after a draw ratio of 10.77, highly crystalline polyethylene is obtained (see Figure 1d). After the NPT equilibration runs at 300 K, the lengths of the polyethylene crystal usually change slightly due the release of the residual stress. Red asterisks in Figure 2a indicate the stretched lengths (with stress) at 500 K with arrows pointing to the equilibrium lengths (without stress) at 300 K. The thermal conductivities of the equilibrated structures are then calculated at 300 K using nonequilibrium molecular dynamics (NEMD) (see the Method section and section 2 in the Supporting Information for details). Figure 2a shows that the thermal conductivity increases significantly from 0.3 to 52.9 W/mK after the amorphous polyethylene is drawn into highly ordered crystalline structures, demonstrating a ~176-fold increase in the thermal conductivity. We have also tested different drawing rates from 32 to 432 m/s. We find that the drawing rates do not influence the calculated thermal conductivities.

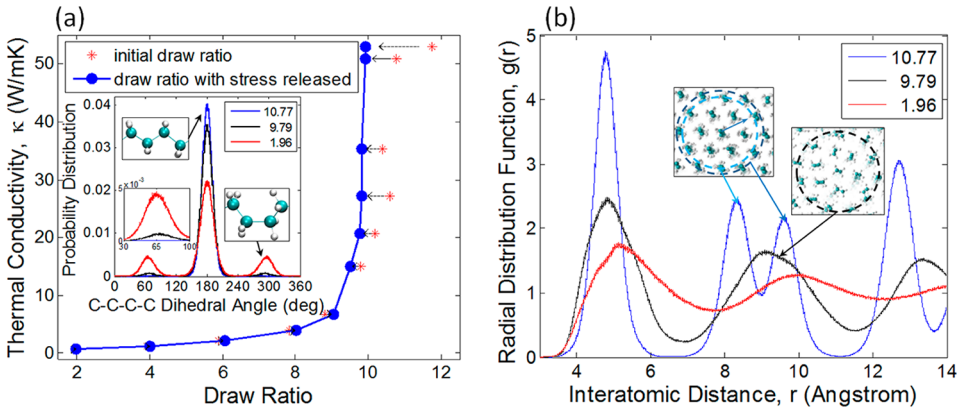

Figure 2. (a) Thermal conductivity of crystalline polyethylene after the drawing process with different draw ratios. In general, after the residual stress is released after drawing to different draw ratios, the final draw ratios (blue dots) are different from the initial ones (red asterisks). Inset in panel (a) shows the probability distribution of the dihedral angle of the polyethylene backbone. The sharp monopeak in the dihedral angle distribution of chains with large draw ratios indicates less segmental rotation and better lattice order along the chains. (b) Interchain radial distribution functions (RDFs) of polyethylene with different draw ratios characterize the relative positions of carbon atoms in a cross-sectional plane. As the draw ratio is increased, peaks shift to smaller values, indicating a more compact interchain structure. The splitting of the peak around 8−10 Å shows that large draw ratio can improve interchain order. Insets in panel (b) visualize the structure change due to different draw ratios and the radii corresponding to the peaks.

To correlate the thermal conductivity with the morphology, we characterize the structure by calculating the probability distribution of the dihedral angle of the polyethylene backbone (see inset of Figure 2a). The distribution shows that a sharp monopeak at 180°, indicating an *all-trans* conformation, will replace the broader multipeak feature, which suggests a mixture of *trans* (180°) and *gauche* (60 and 300°) conformations, as the polymer is stretched longer. This means that the CH_2 segments along a chain are more ordered and there are less segmental rotations. The chains with better along-chain segmental order will pose less disorder scattering to phonons and thus have higher thermal conductivity.

Besides the along-chain order, the interchain structure also undergoes significant morphology changes during the drawing process (see Figure 2b). Interchain radial distribution function (RDF) of carbon atoms is used to characterize the cross-sectional lattice structure. Taking one carbon atom (x_0, y_0, z_0) as the reference atom, its distance to other carbon atoms in the cross-sectional plane is calculated as $R = ((y - y_0)^2 + (z - z_0)^2)^{1/2}$. To suppress noise in the data, only carbon atoms within a narrow spatial interval in the chain-length direction, $|x - x_0| < 1$ Å, are considered. Then, interchain RDF is calculated using $g(r) = n/2\pi r\rho l$, where n is the number of carbon atoms satisfying $r < R < r + dr$, ρ is the average number density of carbon atom, and l is the slice thickness in the x-direction (2 Å). As the draw ratio increases from 1.96 to 10.77, a more compact structure is formed, indicated by peaks shifting to smaller r. For the structure obtained from the lowest draw ratio of 1.96, the peaks are broad and have overlaps (red line in Figure 2b). As the draw ratio increases, peaks become sharper and more separated, suggesting the formation of ordered lattice (black and blue lines in Figure 2b). The peak at 8−10 Å (black line, Figure 2b) of the polyethylene with the draw ratio of 9.79 further split into two sharp peaks (blue line, Figure 2b) when the draw ratio is increased to 10.77. By observing the structures with these two draw ratios (insets in Figure 2b), we can see a clear phase change with the structure with a draw ratio of 10.77 being more ordered. This results in a 3.4 times difference in the thermal conductivities of the two corresponding structures. This sudden change in phase is the basis of the thermal conductivity regulation presented in this paper.

The structural and physical properties of ultradrawn polyethylene fibers have been widely studied.[27,28] Polyethylene fibers and bulk polyethylene crystal exhibit complicated phase transition behaviors, and several thermal events happen below the melting point.[29] Our previous work has shown that the phase transition around 400 K can lead to a significant thermal conductivity reduction in crystalline polyethylene.[13] We further narrow down the temperature sampling interval and find that the phase transition happens between 396 and 398 K (Figure 3a). It is worth noting that this phase transition temperature is much lower than the thermal decomposition temperature of ~700 K[30] and the thermo-oxidative decomposition temperature of ~510 K.[31] This phase change leads to a thermal conductivity change by around 5 times (Figure 3a).

We found that such a temperature-induced phase transition is not influenced by the simulation size. However, the thermostats imposed at the two ends of the simulation domain in NEMD will scatter phonons artificially and thus impose a limit to the phonon mean free path in the simulations. We study this finite size effect on thermal conductivity by enlarging the supercell dimension in the chain-length direction. For the

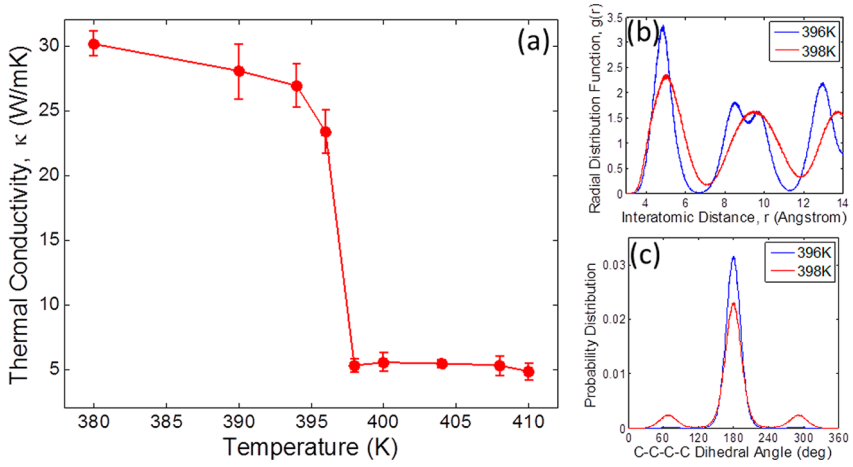

Figure 3. (a) Thermal conductivity of ordered polyethylene from 380 to 410 K. The thermal conductivity of the crystalline polyethylene drops by ~80% from 380 to 400 K. (b) Interchain RDFs and (b) probability distribution of dihedral angles show that both interchain and along-chain lattice orders are experiencing dramatic change around the phase transition temperature.

all-trans structures, we find an increase in the thermal conductivity as the supercell size increases. The thermal conductivity increases from 48.22 to 70.04 W/mK as the supercell size increases from 50 nm (400 CH_2 per chain) to 400 nm (3200 CH_2 per chain) (see section 2 in the Supporting Information). However, the thermal conductivity above the phase change temperature is not influenced by the supercell size, likely due to the short phonon mean free path in the disordered structure. *As a result, real thermal conductivity switching factors should be even larger than those reported here.* However, due to limited computational resources, it is impractical for us to perform all simulations on very large supercells.

Due to phase transition, the along-chain order of the polymer segments and the interchain lattice undergo significant changes within the temperature window of 396−398 K.[27,32] Interchain RDFs (Figure 3b) at these two temperatures show that the interchain lattice experiences almost the same phase change as seen in the drawing process (Figure 2b). Accompanying this interchain lattice phase change, the segmental rotations of the CH_2 segments along the chain increase as indicated in the dihedral angle distributions at different temperatures (Figure 3c)—a feature also observed in the drawing process (inset in Figure 2a).

To characterize the dynamics of the segmental rotation, we calculate the autocorrelation function of the dihedral angle vector, $\vec{\Theta}_d = (\cos\theta_d, \sin\theta_d)$, in the form of a second Legendre polynomial, P_2:

$$P_2(t) = \frac{3}{2}\langle \vec{\Theta}_d(t)\cdot\vec{\Theta}_d(0)\rangle^2 - \frac{1}{2} \qquad (1)$$

From 382 to 408 K, the decay of the correlation function becomes slower with the corresponding relaxation time constant increasing from 2.1 to 8.4 ps according to exponential fits (Figure 4a). Around the phase change temperature, the relaxation time constant increases dramatically from 4.4 to 7.8 ps, although the temperature only increases by 4 K (from 396 to 400 K). In this case, two factors can lead to changes in the decay time constant: temperature and morphology. If the structure stays as a perfect lattice in which atoms only vibrate around the equilibrium positions, due to faster atomic vibrations at higher temperatures, the decay time should be shorter at higher temperatures. The large discontinuity in decay times from 396 to 400 K suggests slower drift motion of segments which rotates more freely due to larger interchain spacing in the less ordered phase, as shown in Figure 2b. Below the phase transition temperature, the autocorrelation functions decay to values larger than 0.9, indicating that the variations of the dihedral angles are largely confined (if there is no variation at all, autocorrelation should remain as 1). Above the phase transition temperature, the autocorrelation functions decay to much smaller values, suggesting that the rotational degrees of freedom can sample a much larger phase space.

We further link the temperature with the chain conformation by calculating the mean-squared radius of gyration of polyethylene chain backbone. The normalized parallel and perpendicular components of the mean-squared radius of gyration are calculated as

$$\langle R_{g||}^2\rangle = \left\langle \frac{\sum_{i=1}^{n}(x_i - x_c)^2 + \sum_{i=1}^{n}(y_i - y_c)^2}{\sum_{i=1}^{n}(r_i - r_c)^2} \right\rangle \qquad (2)$$

$$\langle R_{g\perp}^2\rangle = 1 - \langle R_{g||}^2\rangle \qquad (3)$$

where (x_c, y_c, z_c) is the center of mass of one polyethylene chain, and (x_i, y_i, z_i) is the position of the ith carbon atom in the chain. Gyration radius values are averaged over all the chains in the simulation domain, and error bars are calculated as the standard deviation

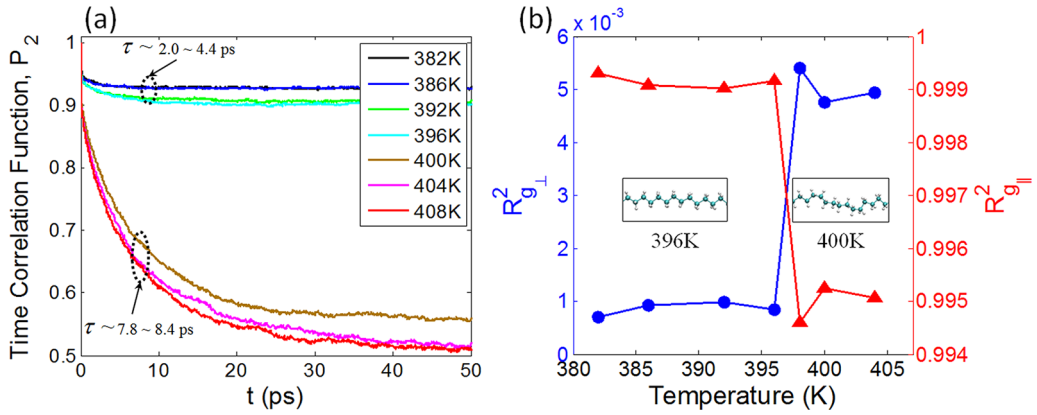

Figure 4. (a) Decay of the autocorrelation function of the dihedral angle vector and (b) radii of gyration of polyethylene chains at different temperatures. As temperature increases from 396 to 400 K, the relaxation time (τ) almost doubles from 4.3 to 7.8 ps. The sudden change in relaxation time from 396 to 400 K indicates a phase transition from a more compact crystalline structure to a less confined structure in which chain segmental rotation is easier. This phase transition alters chain conformation and is further characterized by (b) the mean-squared radii of gyration of polyethylene chains at different temperatures. Parallel gyration radius ($R^2_{g\parallel}$) reflects the span of the chain in the chain-length direction, and perpendicular gyration radius ($R^2_{g\perp}$) is an indication of how straight the segments are aligned. Between 396 and 398 K, discontinuities of chain gyrations show that the along-chain alignment is significantly reduced and chains get more coiled.

of four averaged gyration radii, each of which is obtained from the time averaging of a 0.25 ns run. We decompose the radius of gyration in two directions to characterize the spans of the molecular chains in the cross-sectional plane and the along-chain direction separately. The sudden decrease in $R^2_{g\parallel}$ between 396 and 398 K demonstrates an abrupt shrinkage of the chain length, which is accompanied by the sudden increase in $R^2_{g\parallel}$, which means the chain is no longer straight (Figure 4b). We have also characterized the orientation of the chain segments using Herman's orientation factor[14,33] and find the same sharp change around 397 K (see Figure S12 in the Supporting Information). These phase change effects thus enable sharp switching of thermal conductivity by controlling the temperature.

The thermal conductivity of polyethylene as a function of strain and temperature as shown above can be used for thermal conductivity regulation if the switching is reversible. We thus study the reversibility of the thermal conductivity change influenced by temperature, strains, and their combinations (see section 3 in the Supporting Information for detailed simulation procedure). Starting from the crystalline structures at 300 K, polyethylene is heated to 450 K gradually. After NPT runs at 450 K for structural equilibration, the thermal conductivities are calculated. Then, chains are stretched 10 or 20% longer than the initial length and cooled to 300 K with the strain maintained. After another NPT run without strain to release any residual stress at 300 K, the thermal conductivities are calculated again. We have performed such a cycle for four times and found that the thermal conductivity can be switched between ~4 and ~50 W/mK (blue and black lines in Figure 5a), achieving a tuning factor of ~12 through the combined temperature and strain effects. The cases with 10 and 20% strains show similar tuning factors. We also find that the temperature alone can also regulate thermal conductivity reversibly, yielding thermal conductivities varying from ~4 to ~32 W/mK, achieving a tuning factor of ~8 (red line, Figure 5a). Such thermal conductivity regulation does not show any degradation over the cycles studied. We performed similar simulations with a smaller temperature difference between 450 and 350 K, and the tuning factors achieved are ~7−10 (see section 4 in the Supporting Information for details). It is worth noting that the structures used for thermal conductivity calculations at 300 and 450 K are not influenced by the heating rate or stretching rate because NPT runs are always performed at the corresponding temperature to obtain optimized structures. In our simulations, each cycle has 1.2 ns duration (see Figure S5 in Supporting Information).

In general, higher temperature results in thermal expansion in the cross-plane and thus enlarges the interchain distance, creating more space for chain segmental rotation. The atomic kinetic energy is also larger at higher temperatures, enabling the relatively small dihedral energy barriers to be easily overcome and thus more segmental rotations. Such segmental rotations destroy the lattice order along the molecular chains, introducing significant structural disorders which scatter phonons and decrease thermal conductivity. When temperature decreases, the intermolecular distance decreases, making the chain movement more confined. However, not all the dihedral angles can return to 180° (Figure 5c) by only decreasing the temperature. Applying strain can help reset the dihedral angles, as seen in the reduced shoulder profile in the inset of Figure 5c, thus further increasing the contrast of thermal conductivity switching.

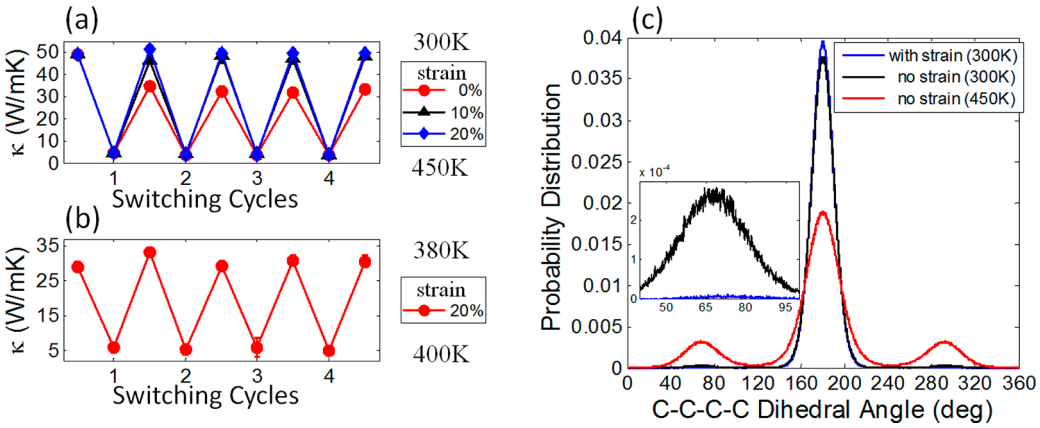

Figure 5. (a) Thermal conductivity switching of crystalline polyethylene between 300 and 450 K with different strains. By controlling temperature and strain, thermal conductivity tuning factors up to ~12 are achieved. (b) For a smaller temperature window of 20 K, the thermal conductivity tuning factor can still be as high as ~6. (c) Dihedral angle distribution for polyethylene crystal at 300 and 450 K. The left inset of panel (c) shows that applying strains can effectively reduce the probability of the dihedral angle being at ~60 and ~300° by resetting *gauche* conformation to *trans* conformation.

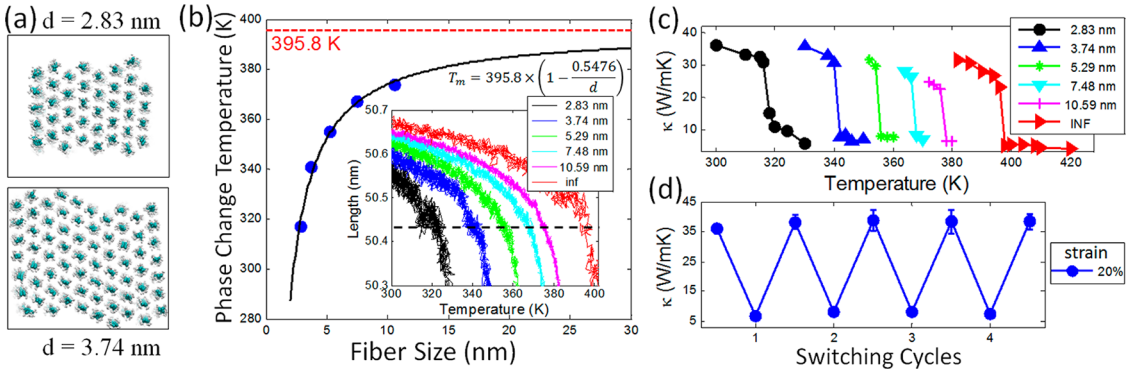

Figure 6. (a) Cross-sectional view of polyethylene fibers with different sizes. (b) Phase transition temperature of polyethylene fibers with different sizes determined by a critical length (inset). (c) Thermal conductivity of polyethylene fibers with different sizes as functions of temperature. (d) Thermal conductivity switching cycles for a 2.83 nm polyethylene fiber.

For practical applications of this thermal conductivity regulation, a relatively narrow temperature window is preferred. We repeated the simulations for the cycles with a 20% strain, but with temperature bounds set to 380 and 400 K. A tuning factor of ~6 is achieved with this 20 K temperature switch, and the reproducibility of this factor is demonstrated (Figure 5b). This tuning factor is about 2-fold higher than that achieved in the solid−liquid phase transition in nanofluids with a similar temperature difference.[7] Morphology change at these temperatures exhibits similar features as those in the 300/450 K case (Figure S7 in Supporting Information). It is worth noting that our high tuning factors are achieved even though there is simulation size effect on the thermal conductivity. As discussed before, the tuning factor can be even larger if larger simulation sizes are used (see section 2 in the Supporting Information).

In order to adapt this thermal conductivity regulation scheme to different applications, it is desirable that the switching temperature can vary. Crystal size is known to influence the melting point of traditional crystalline or semicrystalline polyethylene.[34] Nanofibers have much higher surface to volume ratios, and surface atoms have smaller cohesive energy due to fewer neighboring atoms compared to those inside the material.[35] Due to this reason, nanostructures have lower melting points than that of their bulk counterpart—a phenomenon known as size-dependent melting-point depression.[36,37] The same principle should also apply to the above-mentioned phase change temperature of polyethylene nanofibers. We studied the polyethylene fibers with different sizes by simulating bundles consisting of different numbers of aligned chains surrounded by vacuum in the simulation domain (see Figure 6a for example). The fiber size is calculated as the square root of the fiber cross-sectional area. The cross-sectional area is calculated as the product of the number of chains in the fiber and the cross-sectional area per chain in the crystalline structure optimized at 300 K. The sizes of the polyethylene fibers vary from 2.83 to 10.59 nm. For this set of simulations, we applied periodic boundary conditions only in the chain-length direction (the *x*-direction). Simulations first run in NPT ensembles to obtain

equilibrium structures at 300 K. Fibers are then heated at a rate of 80 K/ns from 300 to 450 K to roughly determine the phase transition temperature for each fiber size. We also tried different heating rates from 80 to 600 K/ns and observed phase transition in all cases.

During phase transition, the cross-sectional areas of the fibers increase dramatically and the length of simulation domain shrinks slightly. Since the exact volumes of the fibers are difficult to calculate due to the irregular cross-sectional shapes, we use the simulation domain lengths, which have been shown to be a function of phase (see Figure 4b), to characterize the phase transition phenomenon. The lengths, initially at 50.52−50.68 nm, will shrink as temperature increases, and the shrinkage will speed up after the lengths are less than 50.43 nm (inset, Figure 6b). The phase change temperature is roughly estimated by locating the temperature at which chains have shrunk to 50.43 nm. Several temperatures around the estimated phase transition temperatures are sampled, and NPT runs are performed at each temperature for 1 ns. After eliminating the influence of heating rate by NPT runs, the morphologies at the sampled temperatures are examined, and the exact phase transition temperatures are determined (Figure 6b). The thermal conductivities are calculated using the stable structures obtained from NPT runs (Figure 6c).

Similar to the crystalline polyethylene, the thermal conductivity of polyethylene nanofibers also decreases as temperature increases, and sharp changes are observed at the phase change temperatures (Figure 6c). Structure characterizations of the polyethylene fibers with sizes of 2.83 and 3.74 nm confirm that the phase transition indeed happens around the switching temperature, and this phase transition is observed within a very narrow 2 K temperature window (see Figures S8 and S9 in the Supporting Information). As the sizes of the nanofibers increase from 2.83 to 10.59 nm, the thermal conductivity switching temperature becomes higher, increasing from 317 to 374 K. We also found that the thermal conductivity switching temperatures for nanofibers of different sizes (Figure 6c) are very close to those determined by monitoring the fiber length change shown in Figure 6b.

It is known that the melting point of nanostructures (T_m) and that of the bulk material (T_{mb}) satisfy the following relation:[38]

$$T_m = T_{mb}\left[1 - A\left(\frac{v_0\gamma}{0.000573T_{mb}}\right)\right] \quad (4)$$

where A is the surface to volume ratio, v_0 is the atomic volume, and γ is the surface energy. For nanowires, $A = 4/d - 2/l$, where d is the characteristic length of the cross section and l is the fiber length.[38] In our simulation, l is infinite due to the periodic boundary condition used in the chain-length direction, and v_0, γ, and T_{mb} are constants for fibers with different sizes. As a result, eq 4 reduces to

$$T_m = T_{mb}\left[1 - \frac{c}{d}\right] \quad (5)$$

where c is a constant determined by v_0, γ, and T_{mb}. We used eq 5 to fit the phase transition temperatures (blue point, Figure 6b) and obtained T_{mb} of 395.8 K, which agrees almost perfectly with the phase transition temperature (∼396−398 K) of crystalline polyethylene, which is equivalent to a fiber with infinite cross-sectional area. Finally, switching cycles with a 20% strain are simulated for the polyethylene nanofiber with a size of 2.83 nm, and the temperature bounds are set to 310 and 330 K. A tuning factor of ∼5 is achieved, and no degradation of the tunability is observed (Figure 6d). Again, if the finite size effect on thermal conductivity can be eliminated, the tuning factor will be even larger (see Figure S3 in the Supporting Information).

CONCLUSION

In summary, we have demonstrated that fully reversible thermal conductivity switching can be achieved using polyethylene nanofibers. Such thermal conductivity change is a result of the phase transition induced by either temperature change, strain, or their combinations. Different phases have different degrees of segmental order along the polyethylene chains. The increased segmental rotation poses structural defects along the chains, leading to disorder phonon scattering and thus reducing thermal conductivity. Even with the finite size effect on the thermal conductivity in the simulations, the thermal conductivity tunability is found to range from 5 to 12, with the largest achieved by combined strain and temperature effects. In real materials, the tuning factors are expected to be even larger. The switching temperature can also be tuned from ∼317 to ∼396 K by engineering the sizes of the nanofibers. Such phase-change-induced, high-contrast, and reversible thermal conductivity switching based on inexpensive polyethylene nanofibers will inspire significant research interest in the field of nanoscale thermal transport control and potentially enable a wide variety of applications.

METHOD

In this work, molecular dynamics (MD) simulations are used to model polyethylene crystalline and fiber structures. The condensed-phased molecular potentials for atomistic simulation studies (COMPASS)[19] is used. The COMPASS force field has been successfully used for thermal transport studies for different polymers including polyethylene.[12,15,39] It can accurately simulate the structural, vibrational, and thermo-physical properties (*e.g.*, phase transition temperature) of polyethylene in both isolated and condensed phases.[14,19]

Nonequilibrium MD (NEMD) is used to calculate the thermal conductivity of polyethylene structures. To establish a nonequilibrium state, two Langevin thermostats[40] are applied at the ends of the simulation domain so as to impose a temperature gradient across the sample (see Figure S2 in the Supporting Information). After steady state is reached, the temperature gradient (dT/dx) is obtained by fitting the linear portion of the temperature profile, and heat flux (J) is calculated using $J = dQ/dt/S$, where dQ/dt is the average of the energy input and output rates in the thermostatted regions, and S is the cross-sectional area. The cross-sectional area per chain is defined as the optimized S of the crystal simulation cell divided by the number of chains in the cell, thus the S of a fiber polyethylene can be calculated by multiplying the number of chains of the fiber. The thermal conductivity (κ) is calculated by Fourier's law, $\kappa = -J/(dT/dx)$. For each simulation, four thermal conductivity values are obtained for different time blocks in the steady state, and the final value is the average of the four values with the error bar being the standard deviation. We have tested different temperature gradients from 0.0081 to 1.8323 K/nm in NEMD. However, no dependence of thermal conductivity on the temperature gradient is observed. As a result, for all the calculations, we choose to set the heat source and sink temperatures 15 K higher and 15 K lower than the average temperature, respectively. The simulations are carried out using the large-scale atomic/molecular massively parallel simulator (LAMMPS).[41] A 0.25 fs time step is chosen due to the presence of fast vibrating hydrogen atoms. More details of the simulation can be found in the Supporting Information.

Conflict of Interest: The authors declare no competing financial interest.

Acknowledgment. This research was supported in part by the Notre Dame Center for Research Computing and NSF through TeraGrid resources provided by SDSC Trestles under grant number TG-CTS100078. The authors acknowledge the financial support from the University of Notre Dame.

Supporting Information Available: Molecular dynamics simulation setup, finite size effect on thermal conductivity, simulation procedure for reversibility study, thermal conductivity switching with narrow temperature boundaries, additional structural and dynamic characterization for crystalline and fiber polyethylene, and chain orientation characterization by Herman's orientation factors. This material is available free of charge *via* the Internet at http://pubs.acs.org.

REFERENCES AND NOTES

1. Supino, R. N.; Talghader, J. J. Electrostatic Control of Microstructure Thermal Conductivity. *Appl. Phys. Lett.* **2001**, *78*, 1778–1780.
2. Laws, A. D.; Chang, Y. J.; Bright, V. M.; Lee, Y. C. Thermal Conduction Switch for Thermal Management of Chip Scale Atomic Clocks (IMECE2006-14540). *J. Electron. Packag.* **2008**, *130*, 021011.
3. Kim, H. S.; Liao, H. H.; Song, H. O.; Kenny, T. W. Variable Thermal Resistors (VTR) for Thermal Management of Chip Scale Atomic Clocks (CSAC). *IEEE Int. Conf. MEMS* **2008**, 852–855.
4. He, J. H.; Singamaneni, S.; Ho, C. H.; Lin, Y.; McConney, M. E.; Tsukruk, V. V. A Thermal Sensor and Switch Based on a Plasma Polymer/ZnO Suspended Nanobelt Bimorph Structure. *Nanotechnology* **2009**, *20*, 065502.
5. Geng, X.; Patel, P.; Narain, A.; Meng, D. D. A Self-Adaptive Thermal Switch Array for Rapid Temperature Stabilization under Various Thermal Power Inputs. *J. Micromech. Microeng.* **2011**, *21*, 085018.
6. Philip, J.; Shima, P. D.; Raj, B. Nanofluid with Tunable Thermal Properties. *Appl. Phys. Lett.* **2008**, *92*, 043108.
7. Zheng, R.; Gao, J.; Wang, J.; Chen, G. Reversible Temperature Regulation of Electrical and Thermal Conductivity Using Liquid–Solid Phase Transitions. *Nat. Commun.* **2011**, *2*, 289.
8. Chang, C. W.; Okawa, D.; Garcia, H.; Yuzvinsky, T. D. Tunable Thermal Links. *Appl. Phys. Lett.* **2007**, *90*, 193114.
9. Sperling, L. H. *Introduction to Physical Polymer Science*; John Wiley & Sons, Inc.: Hoboken, NJ, 2005.
10. Fujishiro, H.; Ikebe, M.; Kashima, T.; Yamanaka, A. Thermal Conductivity and Diffusivity of High-Strength Polymer Fibers. *Jpn. J. Appl. Phys.* **1997**, *36*, 5633–5637.
11. Shen, S.; Henry, A.; Tong, J.; Zheng, R.; Chen, G. Polyethylene Nanofibres with Very High Thermal Conductivities. *Nat. Nanotechnol.* **2010**, *5*, 251–255.
12. Henry, A.; Chen, G.; Plimpton, S. J.; Thompson, A. 1D-to-3D Transition of Phonon Heat Conduction in Polyethylene Using Molecular Dynamics Simulations. *Phys. Rev. B* **2010**, *82*, 144308.
13. Zhang, T.; Luo, T. Morphology-Influenced Thermal Conductivity of Polyethylene Single Chains and Crystalline Fibers. *J. Appl. Phys.* **2012**, *112*, 094304.
14. Liu, J.; Yang, R. Tuning the Thermal Conductivity of Polymers with Mechanical Strains. *Phys. Rev. B* **2010**, *81*, 174122.
15. Luo, T.; Esfarjani, K.; Shiomi, J.; Henry, A.; Chen, G. Molecular Dynamics Simulation of Thermal Energy Transport in Polydimethylsiloxane. *J. Appl. Phys.* **2011**, *109*, 074321.
16. Liu, J.; Yang, R. Length-Dependent Thermal Conductivity of Single Extended Polymer Chains. *Phys. Rev. B* **2012**, *86*, 104307.
17. Pal, S.; Balasubramanian, G.; Puri, I. K. Reducing Thermal Transport in Electrically Conducting Polymers: Effects of Ordered Mixing of Polymer Chains. *Appl. Phys. Lett.* **2013**, *102*, 023109.
18. Shin, S.; Kim, H. K.; Song, J.; Choi, D. J.; Cho, H. H. Phase-Dependent Thermal Conductivity of $Ge_1Sb_4Te_7$ and N: $Ge_1Sb_4Te_7$ for Phase Change, Memory Applications. *J. Appl. Phys.* **2010**, *107*, 033518.
19. Sun, H. COMPASS: An *Ab Initio* Force-Field Optimized for Condensed-Phase Applications—Overview with Details on Alkane and Benzene Compounds. *J. Phys. Chem. B* **1998**, *102*, 7338–7364.
20. Sundararajan, P. R.; Kavassalis, T. A. Molecular Dynamics Study of Polyethylene Chain Folding: The Effects of Chain Length and the Torsional Barrier. *J. Chem. Soc., Faraday Trans.* **1995**, *91*, 2541–2549.
21. Weber, T. A.; Helfand, E. Molecular Dynamics Simulation of Polymers. I. Structure. *J. Chem. Phys.* **1979**, *71*, 4760–4762.
22. Frenkela, D. Simulations: The Dark Side. *Eur. Phys. J Plus* **2013**, *128*, 10.
23. Jae, Ko, M.; Waheed, N.; Lavine, M. S.; Rutledge, G. C. Characterization of Polyethylene Crystallization from an Oriented Melt by Molecular Dynamics Simulation. *J. Chem. Phys.* **2004**, *121*, 2823–2832.
24. Keller, A. Morphology of Crystallizing Polymers. *Nature* **1952**, *169*, 913–914.
25. Hay, I. L.; Keller, A. Morphology of Synthetic Fibres; A Study on Drawn Polyethylene. *Nature* **1964**, *204*, 862–864.
26. Binsbergen, F. L. Orientation-Induced Nucleation in Polymer Crystallization. *Nature* **1966**, *211*, 516–517.
27. Ratner, S.; Weinberg, A.; Wachtel, E.; Moret, P. M.; Marom, G. Phase Transitions in UHMWPE Fiber Compacts Studied by *In Situ* Synchrotron Microbeam WAXS. *Macromol. Rapid Commun.* **2004**, *25*, 1150–1154.
28. Kwon, Y. K.; Boller, A.; Pyda, M.; Wunderlich, B. Melting and Heat Capacity of Gel-Spun, Ultra-High Molar Mass Polyethylene Fibers. *Polymer* **2000**, *41*, 6237–6249.
29. Wunderlich, B.; Czornyj, G. A Study of Equilibrium Melting of Polyethylene. *Macromolecules* **1977**, *10*, 906–913.
30. Ding, W.; Liang, J.; Anderson, L. L. Thermal and Catalytic Degradation of High Density Polyethylene and Commingled Post-Consumer Plastic Waste. *Fuel Process. Technol.* **1997**, *51*, 47–62.
31. Rudnik, E.; Dobkowski, Z. Thermal Degradation of UHMWPE. *J. Therm. Anal.* **1997**, *49*, 471–475.
32. Tashiro, K.; Sasaki, S.; Kobayashi, M. Structural Investigation of Orthorhombic-to-Hexagonal Phase Transition in Polyethylene Crystal: The Experimental Confirmation of the Conformationally Disordered Structure by X-ray Diffraction and Infrared/Raman Spectroscopic Measurements. *Macromolecules* **1996**, *29*, 7460–7469.

33. Pal, S.; Balasubramanian, G.; Puri, I. K. Modifying Thermal Transport in Electrically Conducting Polymers: Effects of Stretching and Combining Polymer Chains. *J. Chem. Phys.* **2012**, *136*, 044901.
34. Hoffman, J. D.; Weeks, J. J. X-ray Study of Isothermal Thickening of Lamellae in Bulk Polyethylene at the Crystallization Temperature. *J. Chem. Phys.* **1965**, *42*, 4301–4302.
35. Roduner, E. Size Matters: Why Nanomaterials Are Different. *Chem. Soc. Rev.* **2006**, *35*, 583–592.
36. Bertsch, G. Melting in Clusters. *Science* **1997**, *277*, 1619.
37. Zhang, M.; Efremov, M. Y.; Schiettekatte, F.; Olson, E. A.; Kwan, A. T.; Lai, S. L.; Wisleder, T.; Greene, J. E.; Allen, L. H. Size-Dependent Melting Point Depression of Nanostructures: Nanocalorimetric Measurements. *Phys. Rev. B* **2000**, *62*, 10548–10557.
38. Nanda, K. K.; Sahu, S. N.; Behera, S. N. Liquid-Drop Model for the Size-Dependent Melting of Low-Dimensional Systems. *Phys. Rev. A* **2002**, *66*, 013208.
39. Luo, T.; Lloyd, J. R. Enhancement of Thermal Energy Transport Across Graphene/Graphite and Polymer Interfaces: A Molecular Dynamics Study. *Adv. Funct. Mater.* **2012**, *22*, 2495–2502.
40. Schneider, T.; Stoll, E. Molecular-Dynamics Study of a Three-Dimensional One-Component Model for Distortive Phase Transitions. *Phys. Rev. B* **1978**, *17*, 1302–1322.
41. Plimpton, S. Fast Parallel Algorithms for Short-Range Molecular Dynamics. *J. Comput. Phys.* **1995**, *117*, 1–19.